Frontiers of Optoelectronics (2023) 16:31
https://doi.org/10.1007/s12200-023-00083-2

Frontiers of Optoelectronics

RESEARCH ARTICLE

Upconversion luminescence and optical thermometry behaviors of Yb^{3+} and Ho^{3+} co-doped GYTO crystal

Chuancheng Zhang[1] · Shoujun Ding[1,2,3,4] · Miaomiao Wang[1] · Hao Ren[1] · Xubing Tang[1] · Yong Zou[1] · Renqin Dou[2] · Wenpeng Liu[2]

Received: 18 July 2023 / Accepted: 12 September 2023

Abstract

Optical thermometry based on the upconversion (UC) luminescence intensity ratio (LIR) has attracted considerable attention because of its feasibility for achievement of accurate non-contact temperature measurement. Compared with traditional UC phosphors, optical thermometry based on UC single crystals can achieve faster response and higher sensitivity due to the stability and high thermal conductivity of the single crystals. In this study, a high-quality 5 at% Yb^{3+} and 1 at% Ho^{3+} co-doped $Gd_{0.74}Y_{0.2}TaO_4$ single crystal was grown by the Czochralski (Cz) method, and the structure of the as-grown crystal was characterized. Importantly, the UC luminescent properties and optical thermometry behaviors of this crystal were revealed. Under 980 nm wavelength excitation, green and red UC luminescence lines at 550 and 650 nm and corresponding to the $^5F_4/^5S_2 \rightarrow {}^5I_8$ and $^5F_5 \rightarrow {}^5I_8$ transitions of Ho^{3+}, respectively, were observed. The green and red UC emissions involved a two-photon mechanism, as evidenced by the analysis of power-dependent UC emission spectra. The temperature-dependent UC emission spectra were measured in the temperature range of 330–660 K to assess the optical temperature sensing behavior. At 660 K, the maximum relative sensing sensitivity (S_r) was determined to be 0.0037 K^{-1}. These results highlight the significant potential of Yb,Ho:GYTO single crystal for optical temperature sensors.

Keywords Yb,Ho:GYTO · Optical temperature sensor · Luminescence intensity ratio · Upconversion luminescence

1 Introduction

Lanthanide-based upconversion (UC) luminescence is a process that converts low-energy photons (near infra-red, NIR) into high-energy photons (visible) through the anti-Stokes mechanism. This phenomenon offers potential for remarkable applications in various fields, including super-resolution nanomicroscopes, photovoltaic cells, sensing, and detection [1–3]. The advantages of UC luminescence include a low autofluorescence background, excellent photostability and non-contact thermometry [4–6]. Temperature, as a fundamental and significant physical parameter, plays a crucial role in numerous aspects of our lives. Temperature control is essential in experimental settings and manufacturing processes. However, conventional temperature measurement methods, which involve contact, are not suitable for certain fields such as intracellular temperature measurement, and in coalmines or power stations due to harsh conditions [7–9]. Therefore, the development of non-contact thermometry measurements has become an important requirement.

In recent years, non-contact temperature sensing techniques based on rare earth (Re) materials have emerged as a hot topic due to their rapid response and high precision [10, 11]. Among these techniques, the luminescence intensity ratio (LIR) derived from UC luminescence is widely used for non-contact temperature measurements. Traditionally, the LIR technique relies on detecting the thermally coupled two energy levels of rare earth ions [7], such as the well-known

✉ Shoujun Ding
sjding@ahut.edu.cn

✉ Renqin Dou
drq0564@mail.ustc.edu.cn

1 School of Microelectronics and Data Science, Anhui University of Technology, Maanshan 243002, China

2 Anhui Institute of Optics and Fine Mechanics, Chinese Academy of Sciences, Hefei 230031, China

3 Advanced Laser Technology Laboratory of Anhui Province, Hefei 230037, China

4 Anhui Provincial Joint Key Laboratory of Disciplines for Industrial Big Data Analysis and Intelligent Decision, Maanshan 243002, China

Published online: 31 October 2023

Er^{3+}($^2H_{11/2}$, $^3S_{3/2}$) [12] and Tm^{3+}($^3F_{2,3}$, $^3H_4$) [13]. However, the sensitivity of these sensors is limited by the energy gaps between these pairs of levels [14]. As a result, non-thermally coupled energy levels (NTCLs), such as Ho^{3+}($^5F_4$/$^5S_2$ and $^5F_5$ [15]), have gradually gained more attention of researchers. The energy levels of trivalent holmium ions (Ho^{3+}) offer favorable conditions for achieving accurate temperature measurements. The energy gap equating to approximately 3000 cm^{-1} between $^5F_4$/$^5S_2$ and $^5F_5$ allows for distinct emission bands [16, 17]. However, commercially available 980 nm laser diodes (LDs) are not efficient at exciting Ho^{3+} ions [18]. That is why Yb^{3+} co-doping with Ho^{3+} becomes crucial, as Yb^{3+} ions play a vital role in enhancing the emission by Ho^{3+}. Yb^{3+} possesses unique features, including outstanding absorption at 980 nm and favorable energy levels matching with those of Ho^{3+} ions, making it an excellent sensitizer [19–22]. The energy transfer mechanism between Yb^{3+} and Ho^{3+} in α-$NaYF_4$ with strong green emission and in core–shell β-$NaYF_4$ nanoparticles with red emission was investigated by Zhang et al. [23] and Pilch et al. [24]. Additionally, numerous UC luminescent matrices co-doped with Yb^{3+} and Ho^{3+} were thoroughly studied for their potential application in non-thermally coupled temperature sensors based on the LIR technique. The examples of such matrices include $Y_2Ti_2O_7$ [25], $(La_{0.1}Y_{0.9})_2O_3$ [26], Y_2O_3 [27], GaF_2 [28], $KLu(WO_4)_2$ [29] and fluoroborate glasses [30]. The RE tantalate series matrices have witnessed rapid development since their first synthesis by Brixner in 1964 [31]. These matrices offer excellent physical and chemical stability which is extremely valuable [32].

The low symmetry and strong crystal field effect of $GdTaO_4$ (GTO) crystal may lead to a higher probability of electro-dipole transitions which is an attractive property in enhancing the photoluminescence efficiency of Re ions [33]. As a result, the 2.1 μm GTO laser crystal doped with Ho^{3+} and Yb^{3+}/Ho^{3+} co-doped $Gd_xY_{1-x}TaO_4$ (GYTO) crystal with the output wavelength of 2.9 μm have been realized by Zhang et al. [33] and Dou et al. [34]. However, there are scarce reports regarding the UC luminescence and temperature sensor application of Yb^{3+}/Ho^{3+} co-doped GTO or GYTO crystals. The ionic radius of Y^{3+} (0.893 Å) is slightly smaller than that of Gd^{3+} (0.938 Å), and so the introduction of Y^{3+} does not cause significant lattice mismatch or structural changes of GTO. Instead, the impurity Y^{3+} efficiently distorts the local symmetry of Gd^{3+} and tunes the crystal field of GTO [34], further amplifying the merits of this crystal. Therefore, the objective of this paper is to investigate the UC luminescence of Yb^{3+}/Ho^{3+} co-doped GYTO crystal and explore its potential applications in temperature sensing.

2 Experimental section

2.1 Preparation of samples

A high-quality GYTO crystal, co-doped with 5 at% Yb^{3+} and 1 at% Ho^{3+}, was grown in N_2 atmosphere using the Czochralski (Cz) method with the JGD-400 Cz furnace (CETC). The crystal growth utilized raw materials Yb_2O_3, Ta_2O_5, Gd_2O_3, Ho_2O_3, and Y_2O_3, all with a purity of 4N and purchased from Shanghai Aladdin Biochemical Technology Co., Ltd. The growth mechanisms employed in this study were consistent with our previous research [35]. The plate presented in Fig. 1a, with a thickness of 2 mm, was cut from the as-grown crystal and polished. The absence of cracks and inclusions in the plate indicated the exceptional optical quality of the crystal, which is crucial for its application in transmittance and absorption characterization.

2.2 Characterizations

The structural characterization of as-grown crystal was conducted using a Bruker D8 Advance X-ray diffractometer equipped with Cu-Kα radiation ($\lambda = 1.5406$ Å). The diffraction angle (2θ) ranged from 10° to 80° with a step size of 0.02°. Fourier transform infrared (FT-IR) spectra were obtained using a Nicolet 6700 spectrometer. Morphology and element distribution were analyzed using a JSM-6510 scanning electron microscope (SEM). The UC emission spectra were measured using an Omni-λ5028i spectrometer coupled with an Andor DU401-BVF charge coupler. A semiconductor laser with a maximum output power of 10 W at 980 nm (BWT Beijing Ltd.) was employed as an excitation source. Temperature-dependent spectra were recorded using the same spectrometer equipped with a temperature regulator that provided a control precision of 0.5 K.

3 Results and discussion

3.1 Crystal structure

To investigate the phase purity and crystalline nature of the crystal, X-ray diffraction (XRD) and Rietveld refinement were conducted. Figure 1c displays a comparison between the XRD patterns of the crystal and standard card GTO (ICDD#240441 [36]). The diffraction peaks of the sample align closely with those of GTO, indicating the successful attainment of a pure phase GYTO crystal with negligible

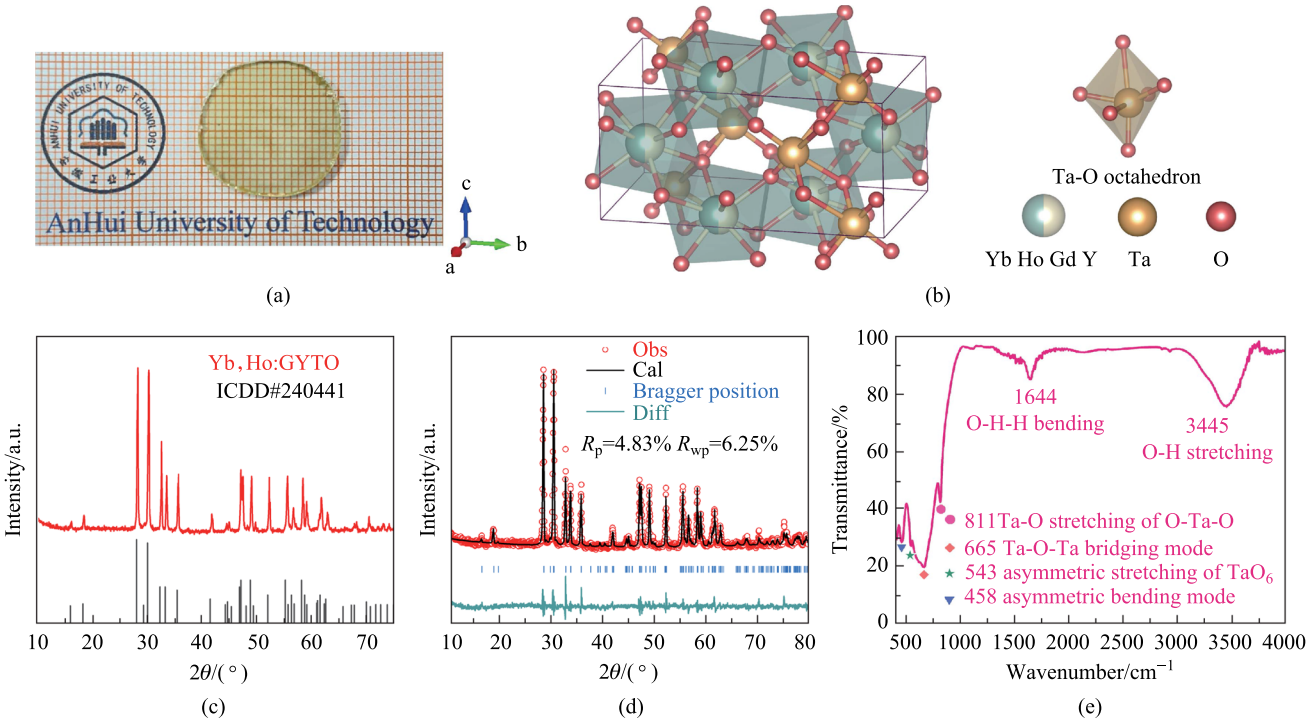

Fig. 1 Structure characterization of Yb,Ho:GYTO crystal: **a** single crystal plate of Yb,Ho:GYTO after cutting and polishing, **b** crystal structure of Yb,Ho:GYTO, **c** XRD pattern of Yb,Ho:GYTO, **d** Rietveld refinement XRD patterns of Yb,Ho:GYTO and **e** the FT-IR spectra of Yb,Ho:GYTO crystal

Table 1 Rietveld refined structural parameters of the Yb,Ho:GYTO crystal

Formula	Yb^{3+},Ho^{3+}:$Gd_{0.74}Y_{0.2}TaO_4$
Crystal system	Monoclinic
Space group	*I* 2/*a*
Cell parameters	$a=5.385(1)$ Å, $b=11.031(3)$ Å, $c=5.080(4)$ Å $\alpha=\gamma=90°$, $\beta=95.5792°$
Reliability	$R_p=4.83\%$, $R_{wp}=6.25\%$, $\chi^2=3.02$

impurities. For a more in-depth analysis of the unit cell parameters and for coordination of the crystal, Rietveld refinement was performed using the Fullprof software. An initial model of M-type GTO was employed. The refined patterns and main crystallographic parameters can be observed in Fig. 1d and Table 1, respectively. It is worth emphasizing that the ionic radii of Y^{3+} (0.90 Å), Yb^{3+} (0.85 Å), and Ho^{3+} (0.89 Å) are all smaller than that of Gd^{3+} (0.93 Å). Consequently, the actual unit cell parameters of the as-grown crystal were expected to be smaller than those of GTO crystal ($a=5.405\pm0.002$ Å, $b=11.063\pm0.007$ Å, $c=5.084\pm0.005$ Å) [37] in theory. The refined results unambiguously confirm this conclusion. The reliability coefficients, $R_p=4.83\%$ and $R_{wp}=6.25\%$, indicate that the crystal exhibits a monoclinic phase (M-type), with Ta^{3+} coordinated by six O^{2-} ions, forming a distorted octahedron [38]. The crystal structure, drawn in Fig. 1b, as created using VESTA software, reveals that the Gd^{3+}, Y^{3+}, Yb^{3+}, and Ho^{3+} ions are randomly distributed on the 4e Wyckoff site, and this leads to the distortion of local crystal filed of Gd^{3+} and effectively enhances the luminescence of Ho^{3+}. The FT-IR spectrum provides a reliable method for determining phonon energy and unveiling various structural details of samples. In Fig. 1e, the FT-IR spectra of Yb,Ho:GTYO crystal is presented. The four characteristic peaks observed at 811, 665, 543, and 458 cm^{-1} are consistent with those reported of $GdTaO_4$ in Ref. [39]. This further corroborates the fact that the as-grown crystal is of a pure monoclinic phase structure.

To ascertain the composition of Yb,Ho:GYTO, SEM was employed, and the resulting element mapping photos are given in Fig. 2. The presence of characteristic peaks corresponding to Gd, Y, Ta, and O in the EDS images confirms the successful growth of GYTO crystal. Analysis of the mapping images unambiguously identifies the presence of Yb, Ho, Gd, Ta, Y, and O elements uniformly distributed throughout the sample.

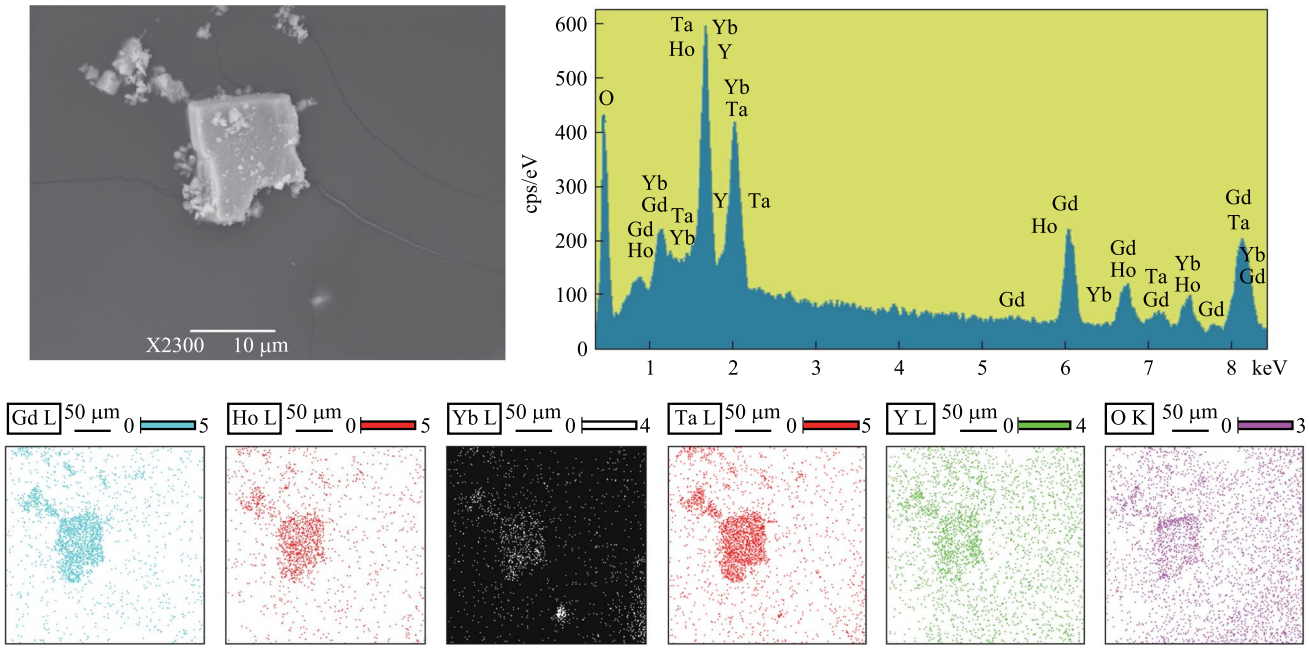

Fig. 2 SEM, EDS images and elemental mapping images of Yb,Ho:GYTO

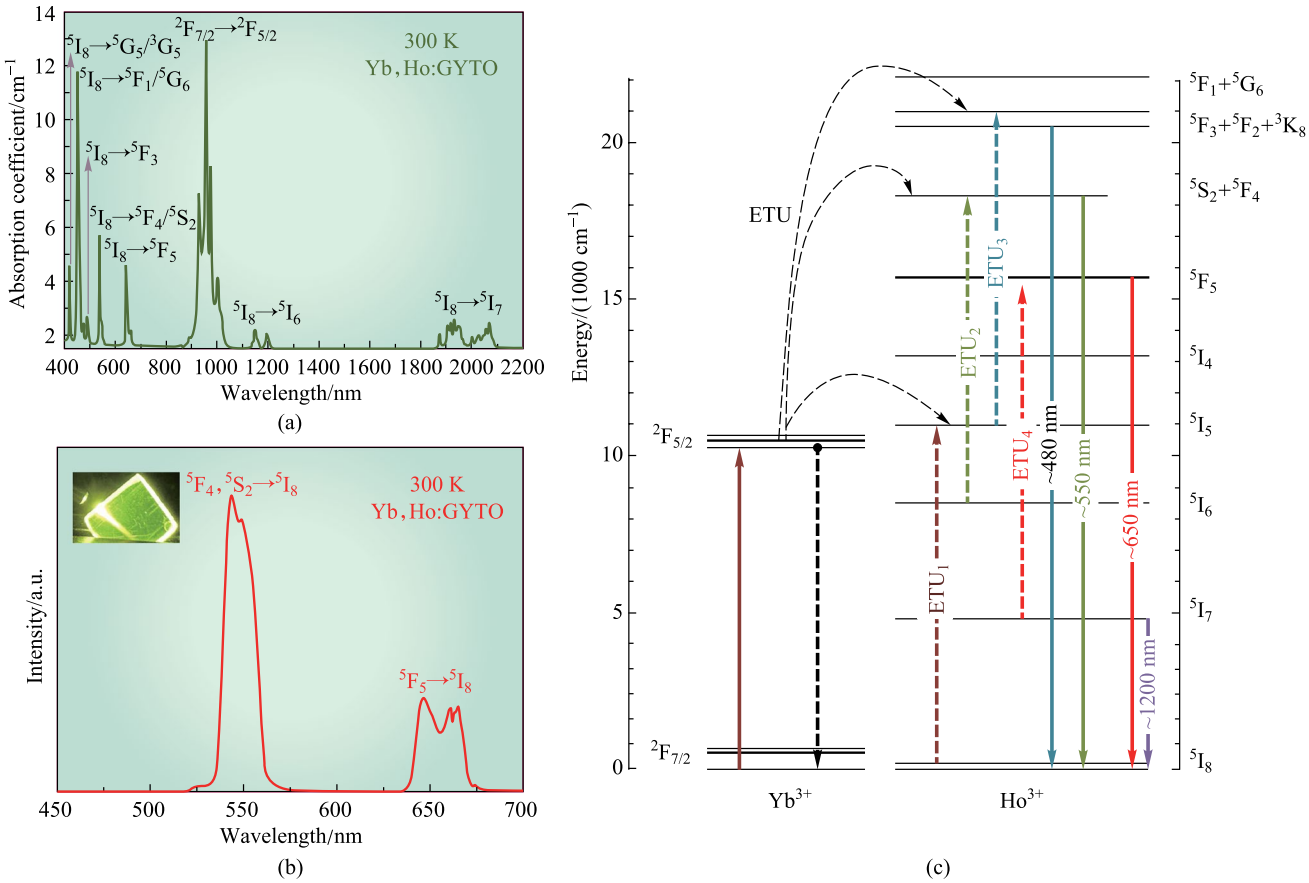

Fig. 3 Room temperature spectroscopic properties of Yb,Ho:GYTO crystal: **a** room temperature absorption spectrum, **b** room temperature emission spectrum and **c** the energy levels of Yb and Ho and the possible UC processes

3.2 Upconversion luminescence

The absorption spectra of Yb,Ho:GYTO in the range of 400–2200 nm at room temperature are shown in Fig. 3a. Among the eight peaks observed, the most prominent and broadest peak is located at 957 nm, which corresponds to the characteristic absorption of Yb^{3+} and corresponds to the $^2F_{7/2} \rightarrow {}^2F_{5/2}$ transition. This absorption band is well aligned with the commercially available InGaAs LD. Additionally, the broad absorption band facilitates improved pumping efficiency and reduced temperature dependence of the pumping source. The remaining peaks, found at 1931, 1150, 642, 539, 487, 450, and 419 nm, can be attributed to the transitions of Ho^{3+} ($^5I_8 \rightarrow {}^5I_7$, $^5I_8 \rightarrow {}^5I_6$, $^5I_8 \rightarrow {}^5F_5$, $^5I_8 \rightarrow {}^5F_4/{}^5S_2$, $^5I_8 \rightarrow {}^5F_3$, $^5I_8 \rightarrow {}^5F_1/{}^5G_6$, $^5I_8 \rightarrow {}^5G_5/{}^3G_5$) [40–42]. The efficiency of UC is significantly influenced by the rate of multiphonon nonradiative relaxation (MNR), represented by W_{NR}, and can be expressed as [43]

$$W_{NR} \propto \left[1 - \exp\left(-\frac{\hbar w}{k_B T}\right)\right]^{-P}, \tag{1}$$

where k_B, $\hbar w$, T, and P are the Boltzmann constant, the phonon energy of the matrix, the absolute temperature, and the number of phonons to complement MNR, respectively. The P value can be calculated by

$$P = \frac{\Delta E}{\hbar w}. \tag{2}$$

These two formulas indicate that smaller MNR always follows the matrix with lower phonon energy. The quite low phonon energy of GTO (~ 345 cm^{-1} [44]) which is comparable with that of tetrafluoride (~ 350 cm^{-1} [45]) is conducive to achieving lower MNR. In this way, the Ho^{3+} ions in GYTO matrix may be of great potential for reaching higher UC luminescence efficiency.

The room temperature UC emission spectra of Yb,Ho:GYTO crystal under 980 nm excitation are presented in Fig. 3b. The inserted image clearly shows a remarkable green emission that is visible to the naked eye. The green emission at approximately 550 nm and the red emission at 650 nm correspond to characteristic transitions of Ho^{3+}: $^5F_4/{}^5S_2 \rightarrow {}^5I_8$ and $^5F_5 \rightarrow {}^5I_8$, respectively [20, 46, 47]. Previous studies [23, 26] have extensively investigated the phenomenon of concentration quenching in UC emission, primarily attributed to an excessive concentration of Yb^{3+}. In these studies, it was shown that, when the concentration of Yb^{3+} exceeds 10 at%, the concentration quenching becomes evident, leading to a significant decrease in UC emission. To avoid such quenching effects and ensure the highest energy transfer efficiency between Yb^{3+} and Ho^{3+}, we controlled the concentration of Yb^{3+} at approximately 5 at%. In Fig. 3c, the energy levels of Yb^{3+} and Ho^{3+} are illustrated to elucidate the UC emission mechanism. Employment of ground-state absorption (GSA) with InGaAs LD, Yb^{3+} achieves population inversion. Subsequently, the UC emission of Ho^{3+} is realized through consecutive energy transfer with the assistance of photons (ETU). In the case of the strong green emission resulting from the $^5S_2/{}^5F_4 \rightarrow {}^5I_8$ transition of Ho^{3+}, the ground state $^5I_8$ is excited to $^5F_3/{}^5F_2/{}^3K_8$ through ETU_1 and ETU_3, $^2F_{5/2}(Yb^{3+}) + {}^2F_{5/2}(Yb^{3+}) + {}^5I_8(Ho^{3+}) \rightarrow {}^5F_3/{}^5F_2/3K_8(Ho^{3+}) + {}^2F_{7/2}(Yb^{3+}) + {}^2F_{7/2}(Yb^{3+})$. These ions then relax to the $^5S_2/{}^5F_4$ level via nonradiative relaxation (NR). Additionally, the ions in the $^5S_2/{}^5F_4$ level may also originate from those at the $^5I_6$ level, which relaxes from $^5I_5$ then accepting energy from another Yb^{3+} through ETU_2 $^2F_{5/2}(Yb^{3+}) + {}^5I_6(Ho^{3+}) \rightarrow {}^5S_2/{}^5F_4(Ho^{3+}) + {}^2F_{7/2}(Yb^{3+})$. The red emission arises from further NR of $^5I_6$ to the $^5I_7$ level, followed by excitation to $^5F_5$ through ETU_4 $^2F_{5/2}(Yb^{3+}) + {}^5I_7(Ho^{3+}) \rightarrow {}^5F_5(Ho^{3+}) + {}^2F_{7/2}(Yb^{3+})$. Finally, the transition from $^5F_5$ to $^5I_8$ generates the red emission centered at 650 nm. In addition, the NR process from the $^5S_2/{}^5F_4$ level to $^5F_5$ of Ho^{3+} ions can also induce this red emission. It should be noted that the energy gaps between $^5S_2/{}^5F_4$ and $^5F_5$, $^5I_6$ and $^5I_7$, are approximately 2931 and 3500 cm^{-1}, respectively [48]. Thus, realizing MNR would require at least 8–10 intrinsic GYTO phonons, which is not realistic. Nonetheless, resonant cross-relaxation (CR) among adjacent Ho^{3+} ions may participate in populating the intermediate energy levels and enhance the populations of $^5S_2/{}^5F_4$ and $^5F_5$ [49].

The emission spectra of this crystal were investigated under 980 nm excitation with varying power in order to further explore the mechanism behind UC emission. Figure 4a clearly shows that the intensity of green and red emissions increases consistently as the pump power increases from 0.1 to 0.5 W. This observation suggests that the population in the $^5F_5$ level of Yb^{3+} effectively enhances the number of excited states of Ho^{3+} through energy transfer upconversion (ETU). Notably, the shape of the emission bands and peak positions remain unchanged. It is well-known that the integrated emission intensity and the pump power serve as valuable indicators for studying the UC luminescence mechanism of Ho^{3+}. Consequently, investigating the absorption processes during the UC mechanism is of utmost importance for gaining a deeper understanding of the luminescence mechanism.

The relationship between integrated intensity I_{up}, pump power P, and the number of photons can be expressed as [50]

$$I_{up} \propto P^n. \tag{3}$$

From this equation, another logarithmic relationship can be deduced

$$\ln I_{up} = n \ln P + C. \tag{4}$$

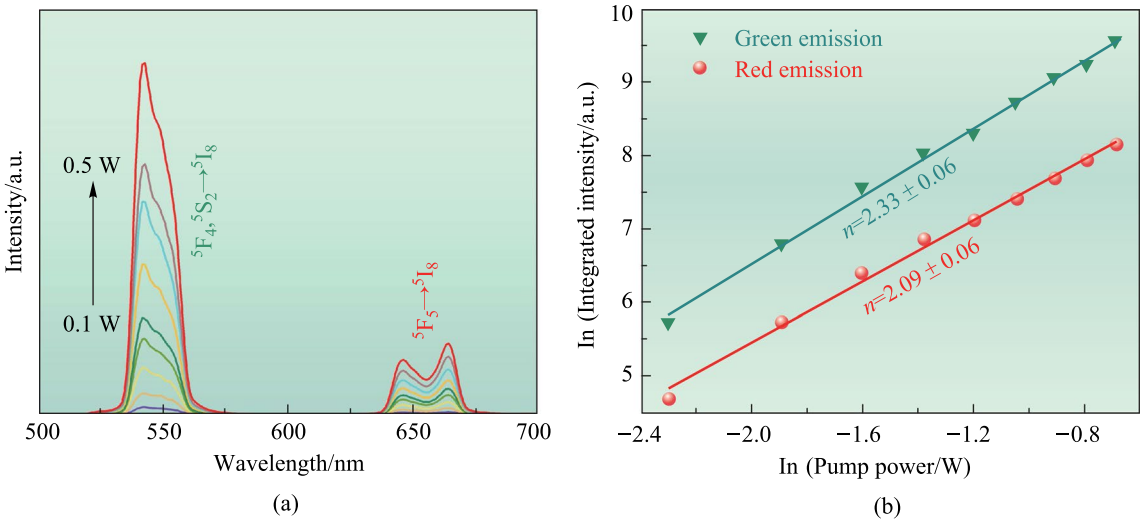

Fig. 4 Power-dependent UC luminescence properties of Yb,Ho:GYTO crystal: **a** UC emission spectra of Yb,Ho:GYTO crystal at different excitation powers and **b** ln–ln plots of pump power dependence of the UC emission intensity

The use of a logarithmic–logarithmic (ln–ln) plot is advantageous for depicting the dependence of UC emission intensity (I_{up}) on the P variable. Figure 4b illustrates that the experimental data can be accurately fitted by a linear function. The values of n for the Yb,Ho:GYTO crystal, corresponding to green and red emissions, are determined to be 2.33 and 2.09, respectively. These values indicate that both the green and red UC emissions adhere to a two-photon mechanism.

3.3 Temperature sensing behavior

To thoroughly investigate the temperature-sensing behavior of Yb,Ho:GYTO crystal, the temperature-dependent non-thermally coupled energy levels (NTCLs) UC emission spectra were meticulously examined. Figures 5a, b display the UC luminescence spectra over the 330–660 K range, clearly demonstrating a consistent decrease of both the green and red emission intensities with increasing temperature. Notably, the decline in green UC emission intensity is more pronounced, as seen in Fig. 5c. This phenomenon is further supported by the observation that the luminescence intensity ratio (LIR) of red and green (I_R/I_G) progressively increases from 330 to 660 K. This effect may arise from the heightened probability of MNR from the $^5S_2/^5F_4$ to $^5F_5$ energy level due to the elevated phonon energy of the crystal with increasing temperature. To elucidate the relationship between red and green emissions, the LIR of both colors is employed. It is important to note that the green and red UC emissions of Ho^{3+} originate from non-thermally coupled energy levels ($^5S_2/^5F_4$ and $^5F_5$); electrons cannot populate the levels through thermal excitation, because of the large energy gaps involved. Therefore, the temperature-dependent LIR can be expressed as [26]

$$\mathrm{LIR}\left(\frac{I_R}{I_G}\right) = A + B \times T + C \times T^2. \tag{5}$$

The formula presented includes constants denoted by A, B, and C, while T represents the absolute temperature. Figure 5c shows the temperature dependence of the LIR for the Ho,Yb:GYTO crystal in the range of 330–660 K. The fitted curve aligns well with the experimental data, revealing an increase in LIR values across the temperature range of 330–660 K. This observation suggests that this crystal has a potential optical thermometry application in wide temperature range. To assess the sensor's performance, further investigation into absolute sensitivity (S_a) and relative sensitivity (S_r) was conducted. The relationship between S_a, S_r, and temperature can be expressed as follows

$$S_a = \left|\frac{d(\mathrm{LIR})}{d(T)}\right|, \tag{6}$$

$$S_r = \left|\frac{d(\mathrm{LIR})}{d(T)}\frac{1}{\mathrm{LIR}}\right|. \tag{7}$$

The S_a and S_r values were calculated using Eqs. (6) and (7), respectively, and the corresponding results are presented in Fig. 5d. It is evident from the figure that S_a exhibits a monotonic increase as the temperature ranges from 330 to 660 K. However, the S_r variation follows a contrasting trend. The maximum values observed for S_a and S_r are 1.03×10^{-3} K at 660 K and 3.67×10^{-3} K at 330 K, respectively. Table 2 provides an overview of the optical

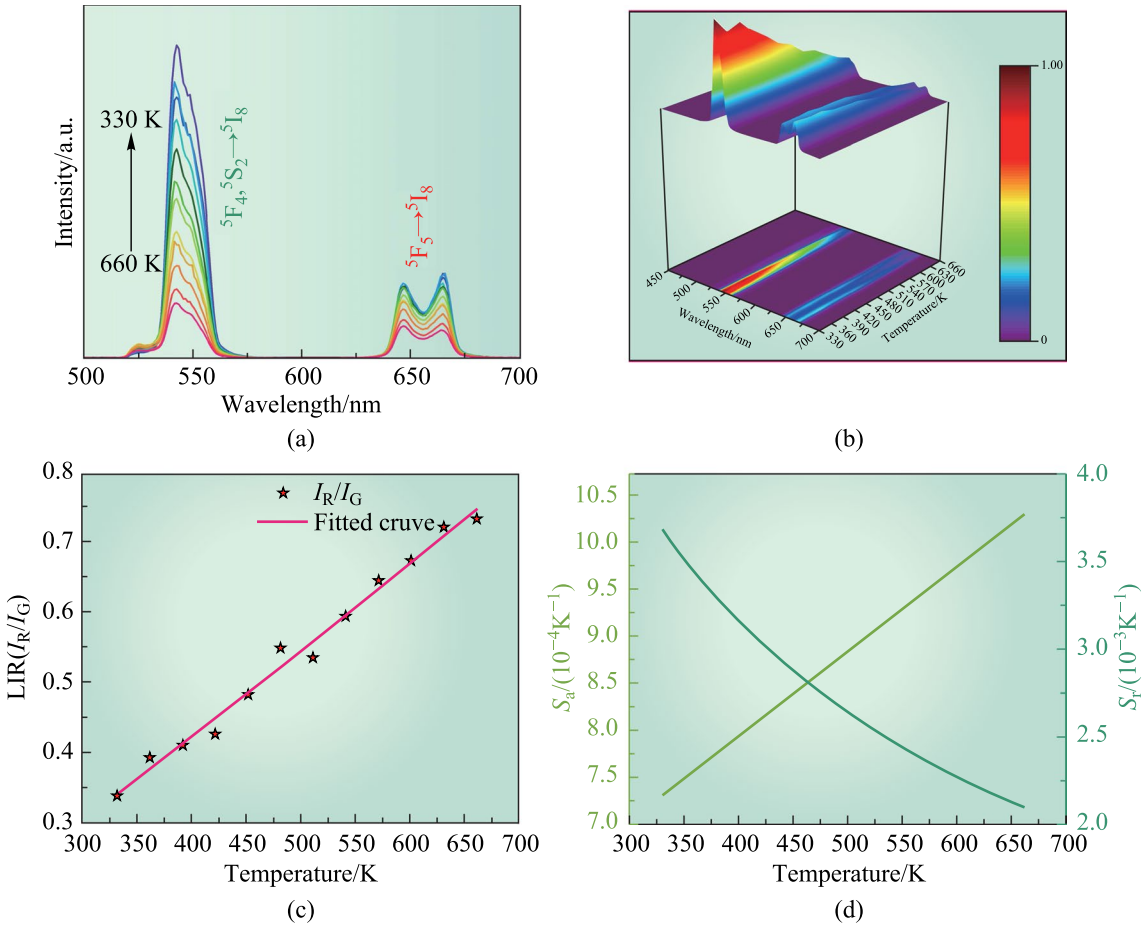

Fig. 5 Temperature sensing behavior of Yb,Ho:GYTO crystal: **a** temperature-dependent UC emission spectra, **b** emission spectrum of Yb,Ho:GYTO at different temperatures (330–660 K), **c** LIR values as a function of temperature ranging from 330 to 660 K and **d** temperature-dependent absolute and relative sensitivity ranging from 330 to 660 K

Table 2 S_r and S_a values of various Yb^{3+}/Ho^{3+} co-doped materials

Materials	S_a/K^{-1}	S_r/K^{-1}	λ_{ex}/nm	ΔT/K	Refs.
Yb^{3+},Ho^{3+}:GYTO	0.0010	0.0037	980	330–660	This work
Yb^{3+},Ho^{3+}:Y_2O_3	–	0.0038	980	293–873	[51]
Yb^{3+},Ho^{3+}:GaF_2	–	0.0030	980	473–713	[52]
Yb^{3+},Ho^{3+}:$KLu(WO_4)_2$	0.0038	0.0054	980	297–673	[53]
Yb^{3+},Ho^{3+}:$Y_2Ti_2O_7$	0.0006	0.0025	980	303–633	[25]
Nd^{3+},Yb^{3+},Ho^{3+}:$LaNbO_4$	–	0.0020	808	303–693	[54]
Yb^{3+},Ho^{3+}:$Sc_2Mo_3O_{12}$	0.0002	0.0085	980	303–573	[55]

thermometry performance of various Yb^{3+}/Ho^{3+} co-doped materials. Notably, this crystal demonstrates excellent temperature sensing capabilities, as indicated by its high S_r value of 3.67×10^{-3} K, surpassing several other Ho^{3+} doped materials, such as Yb^{3+},Ho^{3+}:glass ceramics (1.00×10^{-3} K), Yb^{3+},Ho^{3+}:GaF_2 crystalline powders (3.00×10^{-3} K), and Yb^{3+},Ho^{3+}:$Y_2Ti_2O_7$ nanotubes (2.50×10^{-3} K). Furthermore, this crystal exhibits good thermometric reliability during multiple heating–cooling cycles, as shown in Fig. 6. In total, these findings highlight the crystal's significant potential for application in optical thermometry.

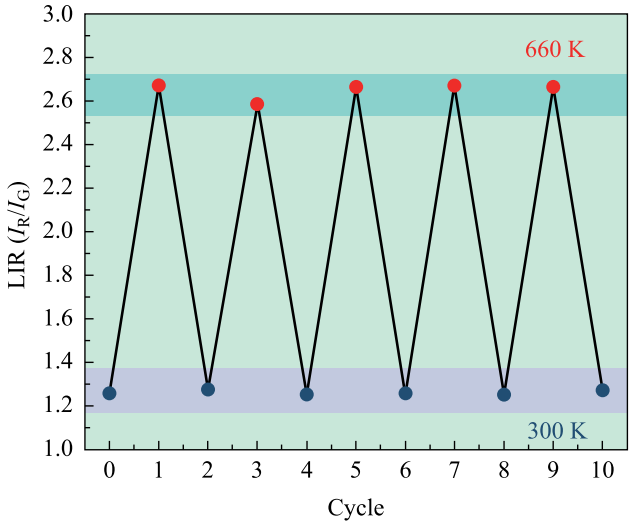

Fig. 6 Thermometer reliability of the crystal during multiple heating–cooling cycles in the temperature range of 300–660 K

4 Conclusion

In summary, the high optical quality Yb,Ho:GYTO crystal was grown using the Cz method. The crystal structure was characterized through X-ray diffraction, Fourier transform infrared spectroscopy and scanning electron microscopy. The results revealed that Yb,Ho:GYTO crystallizes in a Monoclinic (M type) structure with a space group of *I* 2/*a*. The incorporation of Yb^{3+} and Ho^{3+} ions did not alter the GYTO matrix structure type. Notably, when irradiated with a 980 nm LD, a vivid green UC emission was observed with the naked eye. The green and red UC emissions from two non-thermally coupled energy levels in Ho^{3+} were attributed to a two-photon mechanism, as evidenced by the analysis of power-dependent UC emission spectra. The optical temperature sensing capabilities of Yb,Ho:GYTO were investigated using LIR technology and temperature-dependent UC emission spectra. The maximum absolute sensing sensitivity (S_a) and relative sensing sensitivity (S_r) were calculated as 0.0010 and 0.0037 K^{-1}, respectively. These findings highlight the significant potential of Yb,Ho:GYTO for applications in optical thermometry.

Acknowledgements The National Natural Science Foundation of China (Grant No. 52202001), Open Project of Advanced Laser Technology Laboratory of Anhui Province (No. AHL2021KF07), Major Science and Technology of Anhui Province (No. 202203a05020002), University Natural Science Research Project of Anhui Province (No. KJ2021A0388), Natural Science Foundation of Tianjin (No. 20JCYBJC00390), and Chongqing Key Laboratory for Advanced Materials and Technologies of Clean Energy (No. JJNY202001) supported this study.

Author contributions SJ Ding conceived the presented idea. CCZ, MMW and HR carried out the materials preparation and characterization, CCZ, XBT and YZ drafted and revised the manuscript, RQD, WPL and SJD supervised this project. All the authors read and approved the final manuscript.

Availability of data and materials The data that support the findings of this study are available from the corresponding authors, upon reasonable request.

Declarations

Competing interests The authors have no competing interest to disclose.

References

1. Duan, C., Liang, L., Li, L., Zhang, R., Xu, Z.P.: Recent progress in upconversion luminescence nanomaterials for biomedical applications. J. Mater. Chem. B **6**, 192–209 (2018)
2. Zhang, J., Chen, J., Zhang, Y., An, S.: Yb^{3+}/Tm^{3+} and Yb^{3+}/Ho^{3+} doped $Na_9(SiO_4)_6O_2$ phosphors: upconversion luminescence processes, temperature-dependent emission spectra and optical temperature-sensing properties. J. Alloy. Compd. **860**, 158473 (2021)
3. Li, M., Chen, B., Zhang, C., Wang, X., Wu, F., Zhao, R.: Crystallization and up-/down-conversion luminescence of size-dependent $CdWO_4$:Yb^{3+}, RE^{3+} (RE=Ho and Er). Opt. Mater. **142**, 113995 (2023)
4. Wang, J., Su, Q., Lv, Q., Cai, B., Xiaohalati, X., Wang, G., Wang, Z., Wang, L.: Oxygen-generating cyanobacteria powered by upconversion-nanoparticles-converted near-infrared light for ischemic stroke treatment. Nano Lett. **21**, 4654–4665 (2021)
5. Fu, J., Pang, R., Jiang, L., Jia, Y., Sun, W., Zhang, S., Li, C.: A novel dichromic self-referencing optical probe SrO: Bi^{3+}, Eu^{3+} for temperature spatially and temporally imaging. Dalton Trans. **45**, 13317–13323 (2016)
6. Dubey, A., Soni, A.K., Kumari, A., Dey, R., Rai, V.K.: Enhanced green upconversion emission in $NaYF_4$: $Er^{3+}/Yb^{3+}/Li^+$ phosphors for optical thermometry. J. Alloy. Compd. **693**, 194–200 (2017)
7. Zhao, Y., Wang, X., Zhang, Y., Li, Y., Yao, X.: Optical temperature sensing of up-conversion luminescent materials: Fundamentals and progress. J. Alloy. Compd. **817**, 152691 (2020)
8. Wang, C., Jin, Y., Lv, Y., Ju, G., Liu, D., Chen, L., Li, Z., Hu, Y.: Trap distribution tailoring guided design of super-long-persistent phosphor Ba_2SiO_4: Eu^{2+}, Ho^{3+} and photostimulable luminescence for optical information storage. J. Mater. Chem. C **6**, 6058–6067 (2018)
9. Qiao, J., Ning, L., Molokeev, M.S., Chuang, Y.C., Zhang, Q., Poeppelmeier, K.R., Xia, Z.: Site-selective occupancy of Eu^{2+}

toward blue light excited red emission in a $Rb_3YSi_2O_7$: Eu phosphor. Angew. Chem. Chem. **131**, 11645–11650 (2019)
10. Teixeira, R.N., Baratto, A.C.: A Nickel–carbon eutectic cell for contact and non-contact thermometry. Int. J. Thermophys. Thermophys. **28**, 1993–2001 (2007)
11. He, D., Guo, C., Jiang, S., Zhang, N., Duan, C., Yin, M., Li, T.: Optical temperature sensing properties of $Yb3^+$–$Er3^+$ co-doped $NaLnTiO_4$ (Ln= Gd, Y) up-conversion phosphors. (2014)
12. Sun, L.-D., Dong, H., Zhang, P.-Z., Yan, C.-H.: Upconversion of rare earth nanomaterials. Annu. Rev. Phys. Chem. Rev. Phys. Chem. **66**, 619–642 (2015)
13. Cui, S., Chen, G., Chen, Y., Jin, L., Shang, F., Xu, J.: Fabrication, tunable fluorescence emission and energy transfer of Tm^{3+}-Dy^{3+} co-activated P_2O_5–B_2O_3–SrO–K_2O glasses. J. Am. Ceram. Soc. **103**, 1057–1066 (2020)
14. Zhang, J., Ji, B., Chen, G., Hua, Z.: Upconversion luminescence and discussion of sensitivity improvement for optical temperature sensing application. Inorg. Chem. Chem. **57**, 5038–5047 (2018)
15. Liu, S., Cui, J., Jia, J., Fu, J., You, W., Zeng, Q., Yang, Y., Ye, X.: High sensitive Ln^{3+}/Tm^{3+}/Yb^{3+} (Ln^{3+} = Ho^{3+}, Er^{3+}) tri-doped $Ba_3Y_4O_9$ upconverting optical thermometric materials based on diverse thermal response from non-thermally coupled energy levels. Ceram. Int. **45**, 1–10 (2019)
16. Liu, L., Xing, J., Shang, F., Chen, G.: Structure and up-conversion luminescence of Yb^{3+}/Ho^{3+} co-doped fluoroborate glasses. Optics Commun. **490**, 126944 (2021)
17. Tian, Z., Yu, H., Han, Z., Guan, Z., Xu, S., Sun, J., Cao, Y., Wang, Y., Cheng, L., Chen, B.: Luminescence properties, and anti-counterfeiting application of one-dimensional electrospun $Y_2Ti_2O_7$: Ho/Yb nanostructures. Ceram. Int. **48**, 27836–27848 (2022)
18. Kshetri, Y.K., Chaudhary, B., Dhakal, D.R., Murali, G., Pachhai, S., Lee, S.W., Kim, H.-S., Kim, T.-H.: Anomalous upconversion behavior and high-temperature spectral properties of Yb/Ho-SiAlON ceramics. Ceram. Int. **49**, 4807–4815 (2023)
19. Lim, C.S., Aleksandrovsky, A., Molokeev, M., Oreshonkov, A., Atuchin, V.: Structural and spectroscopic effects of Li+ substitution for Na+ in $Li_xNa_{1-x}CaGd_{0.5}Ho_{0.05}Yb_{0.45}(MoO_4)_3$ scheelite-type upconversion phosphors. Molecules **26**, 7357 (2021)
20. Li, H., Zhang, Y., Shao, L., Yuan, P., Xia, X.: Influence of pump power and doping concentration for optical temperature sensing based on $BaZrO_3$: Yb^{3+}/Ho^{3+} ceramics. J. Lumin. Lumin. **192**, 999–1003 (2017)
21. Qi, Y., Li, S., Min, Q., Lu, W., Xu, X., Zhou, D., Qiu, J., Wang, L., Yu, X.: Optical temperature sensing properties of KLu_2F_7: Yb^{3+}/Er^{3+}/Nd^{3+} nanoparticles under NIR excitation. J. Alloy. Compd. **742**, 497–503 (2018)
22. Lim, C.S., Aleksandrovsky, A., Molokeev, M., Oreshonkov, A., Atuchin, V.: The modulated structure and frequency upconversion properties of $CaLa_2(MoO_4)_4$:Ho^{3+}/Yb^{3+} phosphors prepared by microwave synthesis. Phys. Chem. Chem. Phys. **17**, 19278–19287 (2015)
23. Zhang, J.Z., Xia, H.P., Yang, S., Jiang, Y.Z., Xue-mei, G., Zhang, J.L., Jiang, H.C., Chen, B.J.: Upconversion luminescence from Ho^{3+} and Yb^{3+} codoped α-$NaYF_4$ single crystals. Chin. J. Chem. Phys. **28**, 351–354 (2015)
24. Pilch, A., Wurth, C., Kaiser, M., Wawrzynczyk, D., Kurnatowska, M., Arabasz, S., Prorok, K., Samoc, M., Strek, W., Resch-Genger, U., Bednarkiewicz, A.: Shaping luminescent properties of Yb^{3+} and Ho^{3+} Co-doped upconverting core-shell beta-$NaYF_4$ nanoparticles by dopant distribution and spacing. Small **13**, 1701635 (2017)
25. Tian, Z., Yu, H., Han, Z., Guan, Z., Xu, S., Sun, J., Cao, Y., Wang, Y., Cheng, L., Chen, B.: Luminescence properties, and anti-counterfeiting application of one-dimensional electrospun $Y_2Ti_2O_7$:Ho/Yb nanostructures. Ceram. Int. **48**, 27836–27848 (2022)
26. Pan, Y., Lin, H., Hong, R., Zhang, D.: Yb, Ho:$(La_{0.1}Y_{0.9})_2O_3$ ceramics for thermometric applications based on the upconversion emission. J. Luminesc. **238**, 118293 (2021)
27. Pandey, A., Rai, V.K.: Improved luminescence and temperature sensing performance of Ho^{3+}-Yb^{3+}-Zn^{2+}:Y_2O_3 phosphor. Dalton Trans. **42**, 11005–11011 (2013)
28. Rakov, N., Maciel, G.S.: A study of energy transfer phenomenon leading to photon up-conversion in Ho^{3+}:Yb^{3+}:CaF_2 crystalline powders and its temperature sensing properties. Curr. Appl. Phys. Appl. Phys. **17**, 1223–1231 (2017)
29. Savchuk, O.A., Carvajal, J.J., Pujol, M.C., Barrera, E.W., Massons, J., Aguilo, M., Diaz, F.: Ho, Yb:$KLu(WO_4)_2$ nanoparticles: a versatile material for multiple thermal sensing purposes by luminescent thermometry. J. Phys. Chem. C **119**, 18546–18558 (2015)
30. Liu, L., Xing, J., Shang, F., Chen, G.: Structure and up-conversion luminescence of Yb^{3+}/Ho^{3+} co-doped fluoroborate glasses. Opt. Commun.Commun. **490**, 126944 (2021)
31. Brixner, L.H.: A study of the calcium molybdate-rare earth niobate systems. J. Electrochem. Soc.Electrochem. Soc. **111**, 690 (1964)
32. van Eijk, C.W.E.: Inorganic-scintillator development. Nucl. Instrum. Methods Phys. Res. Sect. A **460**, 1–14 (2001)
33. Zhang, W., Li, L., Zhou, S., Gao, H.: Efficient continuous-wave diode-pumped Ho:GTO laser with a pump recycling scheme. J. Russ. Laser Res. **41**, 94–97 (2020)
34. Dou, R., Zhang, Q., Sun, D., Luo, J., Yang, H., Liu, W., Sun, G.: Growth, thermal, and spectroscopic properties of a 2.911 μm Yb, Ho:$GdYTaO_4$ laser crystal. CrystEngComm **16**, 11007–11012 (2014)
35. Ren, H., Ding, S., Li, H., Liu, W., Zou, Y., Han, Y., Zhang, Q.: Growth, structure and upconversion properties of Yb^{3+} and Er^{3+} co-doped $Gd_3Sc_2Al_3O_{12}$ crystal. J. Lumin. Lumin. **251**, 119149 (2022)
36. McIlvried, M.: Penn State University, University Park, Pennsylvania, USA, ICDD Grant-in-Aid (1972)
37. Keller, C.: Über ternäre Oxide des Niobs und Tantals vom Typ ABO_4. Z. Anorg. Allg. Chem. Anorg. Allg. Chem. **318**, 89–106 (1962)
38. Han, B., Xiao, H., Chen, Y., Huang, J., Gong, X., Lin, Y., Luo, Z., Huang, Y.: Polarized spectroscopic properties and 1046 nm laser operation of Yb^{3+}: $Ca_3TaGa_3Si_2O_{14}$ crystal. J. Lumin. Lumin. **251**, 119219 (2022)
39. Brunckova, H., Medvecky, L., Mudra, E., Kovalcikova, A., Girman, V.: Structural properties of gadolinium orthoniobate and orthotantalate thin films prepared by sol–gel method. J. Alloy. Compd. **735**, 1111–1118 (2018)
40. Jiang, T., Tian, Y., Xing, M., Fu, Y., Yin, X., Wang, H., Feng, X., Luo, X.: Research on the photoluminescence and up-conversion luminescence properties of $Y_2Mo_4O_{15}$:Yb, Ho under 454 and 980 nm excitation. Mater. Res. Bull. **98**, 328–334 (2018)
41. Azam, M., Rai, V.K.: Ho^{3+}-Yb^{3+} codoped tellurite based glasses in visible lasers and optical devices: Judd-Ofelt analysis and frequency upconversion. Solid State Sci. **66**, 7–15 (2017)
42. Denisenko, Y.G., Atuchin, V.V., Molokeev, M.S., Wang, N., Jiang, X., Aleksandrovsky, A.S., Krylov, A.S., Oreshonkov, A.S., Sedykh, A.E., Volkova, S.S.: Negative thermal expansion in one-dimension of a new double sulfate $AgHo(SO_4)_2$ with isolated SO_4 tetrahedra. J. Mater. Sci. Technol. **76**, 111–121 (2021)
43. Tanabe, S., Yoshii, S., Hirao, K., Soga, N.: Upconversion properties, multiphonon relaxation, and local environment of rare-earth ions in fluorophosphate glasses. Phys. Rev. B **45**, 4620 (1992)
44. Zhang, Y., Cao, Y., Zhao, Y., Wang, X., Ran, S., Cao, L., Zhang, L., Chen, B.: Optical temperature sensor based on upconversion luminescence of Er^{3+} doped $GdTaO_4$ phosphors. J. Am. Ceram. Soc. **104**, 361–368 (2020)

45. Suyver, J.F., Grimm, J., Van Veen, M., Biner, D., Krämer, K., Güdel, H.-U.: Upconversion spectroscopy and properties of $NaYF_4$ doped with Er^{3+}, Tm^{3+} and/or Yb^{3+}. J. Lumin. Lumin. **117**, 1–12 (2006)
46. Lim, C.S., Atuchin, V.V., Aleksandrovsky, A.S., Molokeev, M.S.: Preparation of $NaSrLa(WO_4)_3$: Ho^{3+}/Yb^{3+} ternary tungstates and their upconversion photoluminescence properties. Mater. Lett. **181**, 38–41 (2016)
47. Lim, C.S., Atuchin, V.V., Aleksandrovsky, A.S., Molokeev, M.S., Oreshonkov, A.S.: Incommensurately modulated structure and spectroscopic properties of $CaGd_2(MoO_4)_4$: Ho^{3+}/Yb^{3+} phosphors for up-conversion applications. J. Alloy. Compd. **695**, 737–746 (2017)
48. Kaminskiĭ, A. A.: Crystalline lasers: physical processes and operating schemes, (No Title) (1996)
49. Gao, W., Zheng, H., Han, Q., He, E., Wang, R.: Unusual upconversion emission from single $NaYF_4$: Yb^{3+}/Ho^{3+} microrods under NIR excitation. CrystEngComm **16**, 6697–6706 (2014)
50. Pollnau, M., Gamelin, D.R., Lüthi, S., Güdel, H., Hehlen, M.P.: Power dependence of upconversion luminescence in lanthanide and transition-metal-ion systems. Phys. Rev. B **61**, 3337 (2000)
51. Xu, W., Gao, X., Zheng, L., Zhang, Z., Cao, W.: Short-wavelength upconversion emissions in Ho^{3+}/Yb^{3+} codoped glass ceramic and the optical thermometry behavior. Opt. Express **20**, 18127–18137 (2012)
52. Guo, Y., Wang, D., He, Y.: Fabrication of highly porous Y_2O_3:Ho, Yb ceramic and its thermometric applications. J. Alloy. Compd. **741**, 1158–1162 (2018)
53. Zhang, J., Zhang, Y., Jiang, X.: Investigations on upconversion luminescence of $K_3Y(PO_4)_2$:Yb^{3+}-$Er^{3+}/Ho^{3+}/Tm^{3+}$ phosphors for optical temperature sensing. J. Alloy. Compd. **748**, 438–445 (2018)
54. Sheng, C., Li, X., Tian, Y., Wang, X., Xu, S., Yu, H., Cao, Y., Chen, B.: Temperature dependence of up-conversion luminescence and sensing properties of $LaNbO_4$:$Nd^{3+}/Yb^{3+}/Ho^{3+}$ phosphor under 808 nm excitation. Spectrochim. Acta Part A Mol. Biomol. Spectrosc. Acta Part A Mol. Biomol. Spectrosc. **244**, 118846 (2021)
55. Liu, W., Xu, S., Lei, L.: Enhancing upconversion of $Sc_2Mo_3O_{12}$:Yb/Ln (Ln = Er, Ho) phosphors by doping Ca^{2+} ions. Opt. Mater. **143**, 114166 (2023)

Chuancheng Zhang received the B.S. degree in Light Source and Illumination from Anhui University of Technology, China. He is pursuing his master degree in Anhui University of Technology. His current research interests are optical crystal growth of rare earth and devices design.

Shoujun Ding is an Associate Professor in the College of Microelectronics and Data Science, and a Principal Investigator in the Anhui University of Technology (AHUT), China. He received the Ph.D. degree in Optics from University of Science and Technology of China. He joined the College of Mathematics & Physics of AHUT in 2018. In 2017-2018, he is a visiting scholar of Utah State University, USA, sponsored by the CSC. Now, he is the director of Research Center for Functional Single Crystals Growth and Devices of AHUT. His research mainly includes the growth techniques of laser crystals and the luminescent physics of rare earths.

Miaomiao Wang received the B.S. degree in Communication Engineering from Fuyang Normal University, China. She is pursuing her master degree in Anhui University of Technology, China. Her current research interests are the growth of rare earth optical crystals and their optical temperature sensing properties.

Hao Ren received the B.S. degree in Light Source and Illumination from Anhui University of Technology, China. He is pursuing his master degree in Anhui Institute of Optics and Fine Mechanics, Chinese Academy of Sciences, China. His current research interests are laser crystal growth of rare earth and phosphors for temperature sensors.

Xubing Tang is an Associate Professor in Anhui University of Technology, China. He received the Ph.D. degree from Chinese Academy of Sciences, China in 2008. He serves as chairman of School of Microelectronics and Data Science in Anhui University of Technology. He specializes in optoelectronic crystal synthesis, the design, detection and application of optoelectronic devices, including light-emitting diodes.

Yong Zou is an Associate Professor in Anhui University of Technology, China. He received the Ph.D. degree from Nanjing University of Aeronautics and Astronautics, China under the guidance of Prof. Hulin Huang in 2018. He specializes in the simulation of thermal conduction in Czochralski method, temperature field design of crystal growth, and heat dissipation design of optoelectronic devices.

Renqin Dou is an Associate Professor in Anhui Institute of Optics and Fine Mechanics (AIOFM), Chinese Academy of Sciences, China. She received the Ph.D. degree in Optics from University of Science and Technology of China. She joined AIOFM in 2017. For ten years, she is engaged in crystal research, includes the growth techniques and the performance analysis of optical functional crystals.

Wenpeng Liu is an associate professor in Anhui Institute of Optics and Fine Mechanics, Chinese Academy of Sciences, China. He received the Ph.D. degree in Optics from Hefei Institute of Physical Sciences, Chinese Academy of Sciences, China. He is currently mainly engaged in the research and development of functional crystal materials and their application technology.